

Chiral symmetry breaking and topological charge of graphene nanoribbons

Hyun Cheol Lee^{*1} and S.-R. Eric Yang^{†2}

¹Department of Physics, Sogang University, Seoul, Korea

²Department of Physics, Korea University, Seoul, Korea

December 12, 2023

Abstract

We explore the edge properties of rectangular graphene nanoribbons featuring two zigzag edges and two armchair edges. Although the self-consistent Hartree-Fock fields break chiral symmetry, our work demonstrates that graphene nanoribbons maintain their status as short-range entangled symmetry-protected topological insulators. The relevant symmetry involves combined mirror and time-reversal operations. In undoped ribbons displaying edge ferromagnetism, the band gap edge states with a topological charge form on the zigzag edges. An analysis of the anomalous continuity equation elucidates that this topological charge is induced by the gap term. In low-doped zigzag ribbons, where the ground state exhibits edge spin density waves, this topological charge appears as a nearly zero-energy edge mode.

1 Introduction

What is a topological charge? One way to define it is through the generation of mass (or gap), which breaks chiral symmetry[1]. This concept can be elucidated using a one-dimensional Dirac equation. In one spatial dimension (and generally for all odd spatial dimensions), the gapless (or massless in the particle physics context) Dirac fermions possess the property of *chirality*. The Lagrangian density of the massless Dirac fermion (see the Appendix

*hyunlee@sogang.ac.kr

†eyang812@gmail.com

for details and conventions) is invariant under *two* kinds of global gauge transformations:

$$\psi \rightarrow e^{i\Lambda}\psi \text{ ordinary, } \psi \rightarrow e^{i\gamma^5\Lambda}\psi \text{ axial or chiral,} \quad (1)$$

where ψ is a Dirac spinor, and $\gamma^5 = \gamma^0\gamma^1$. Chirality is defined to be the eigenvalue of γ^5 , which can take only ± 1 values. According to classical Noether's theorem, these invariances imply the conservation of the corresponding currents (Fermi velocity may be multiplied to the spatial component):

$$j_{\text{ordinary}}^\mu = \bar{\psi}\gamma^\mu\psi, \quad j_{\text{axial}}^{\mu 5} = \bar{\psi}\gamma^\mu\gamma^5\psi. \quad (2)$$

Owing to a special property of gamma matrices in two dimensions, the above two currents can be related by:

$$j^{\mu 5} = -\epsilon^{\mu\nu}j_\nu, \quad (3)$$

where $\epsilon^{\mu\nu}$ is the two-dimensional Levi-Civita symbol with $\epsilon^{01} = 1$. Expressing the Dirac spinor ψ in γ^5 -diagonal basis as $(\psi_R, \psi_L)^t$ ('t' is transpose), the explicit expressions of currents are given by (note that $j_1 = -j^1$, etc.):

$$j^0 = \psi_R^\dagger\psi_R + \psi_L^\dagger\psi_L = j^{1,5}, \quad j^1 = \psi_R^\dagger\psi_R - \psi_L^\dagger\psi_L = j^{0,5}. \quad (4)$$

A mass term for Dirac fermion couples ψ_R and ψ_L . Two independent mass terms (in Hamiltonian) are allowed in the following way:

$$m(\psi_R^\dagger\psi_L + \text{h.c.}) + im'(\psi_R^\dagger\psi_L - \text{h.c.}). \quad (5)$$

The above mass terms break the chiral symmetry explicitly. From the viewpoint of a one-dimensional polyacetylene system, these masses correspond to the even and the odd components of dimerization. In the presence of the mass terms, the continuity equation for the axial current is modified as follows [1, 2]:

$$\partial_\mu j^{\mu 5} = \frac{\partial j^1}{\partial t} + \frac{\partial j^0}{\partial x} = -2(m - im')\psi_R^\dagger\psi_L - 2(m + im')\psi_L^\dagger\psi_R \equiv \mathcal{M}. \quad (6)$$

Eq.(6) remains valid even if the mass parameters depend on coordinates. For slow adiabatic temporal changes, the time derivative of Eq.(6) can be neglected, and we have ($\rho = j^0$ denotes charge density).

$$\frac{\partial \rho}{\partial x} = \mathcal{M}(x). \quad (7)$$

An abrupt step-like change of the mass terms can give rise to a solitonic[3, 4] topological charge[1] accumulated at the soliton location, where

the spectral weight of a soliton is equally divided between conduction and valence bands. More precisely, $\mathcal{M}(x)$ in Eq.(6) corresponds to the topological charge[5, 6] density after subtracting out the trivial vacuum contribution[1]. Then, the integration of Eq.(7) over some interval with endpoints (say, $[-\infty, \infty]$) gives the topological charge Q_{top} associated with the solitonic configuration of mass parameters

$$\rho(\infty) - \rho(-\infty) = \int_{-\infty}^{\infty} dx \mathcal{M}(x) = Q_{\text{top}}. \quad (8)$$

The determination of this topological charge relies on the topological aspects of the mass parameters, defined as $\mathcal{M}(x) = \frac{\partial \theta}{\partial x}$, where the order parameter $\theta(x)$ represents a kink:

$$\theta(x) = \begin{cases} -1/2 & \text{for } x < 0 \\ +1/2 & \text{for } x > 0. \end{cases} \quad (9)$$

In polyacetylene $\theta(x)$ represents dimerization order[4]. However, this topological charge is not necessarily quantized in general circumstances[1]. Then, by Eq.(8), the induced fermion number can be identified with the topological charge Q_{top} of mass parameters, which is in turn determined by their boundary behavior[3].

Our goal in this paper is to try to understand the formation of a topological charge in disorder-free interacting graphene nanoribbons in view of the above statement. In this vein, we note that atomically precise nanoribbons have been recently fabricated [7, 8, 9]. First, let us give a brief introduction to non-interacting graphene nanoribbons. The band structure of a non-interacting zigzag graphene nanoribbon is shown in Fig.1. Graphene nanoribbons[10, 11, 12, 13] consist of A and B sublattices, as seen in the top figure of Fig.2. The A/B sublattice degree of freedom is referred to as the chirality. The chiral transformation[14, 15] on electron operators is implemented by

$$\hat{\mathbf{a}}_i \rightarrow \hat{\mathbf{a}}_i, \quad \hat{\mathbf{b}}_i \rightarrow -\hat{\mathbf{b}}_i, \quad (10)$$

where $\hat{\mathbf{a}}_i$ and $\hat{\mathbf{b}}_i$ are the electron destruction operators of A and B sublattice sites which are similar to the Dirac fermion ψ_R, ψ_L under the action of γ^5 (see the Appendix). Under the transformation Eq.(10), the nearest-neighbor hopping term between A-B sublattices of the tight-binding Hamiltonian of graphene nanoribbon without on-site interaction changes sign, and this is called the chiral symmetry. This chiral symmetry implies a particle-hole symmetry within the energy spectrum, resulting in zero-energy soliton[16, 17] edge states (thus gapless) in the presence of a zigzag edge in non-interacting graphene nanoribbons[18] (refer to Fig.1). Thus, non-interacting

graphene zigzag nanoribbons are deemed a symmetry-protected topological insulator[19]. However, in this scenario without a gap, as defined above, a topological charge does not exist.

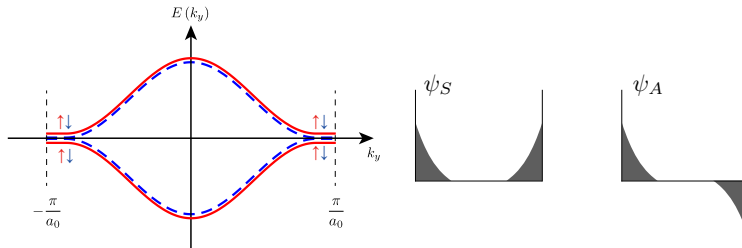


Figure 1: **First:** The band structure of a non-interacting zigzag nanoribbon displays nearly zero-energy states localized on the zigzag edges. **Second:** Solitonic nearly zero-energy states appear near $k = \pm\pi/a_0$, comprising symmetric ψ_B and antisymmetric ψ_A states well-localized on the left and right zigzag edges (a_0 represents the unit cell length of the zigzag ribbon).

Now, the addition of on-site repulsion interaction between electrons explicitly breaks chiral symmetry because the density operator does not change sign under the transformation Eq.(10), and it generates an energy gap Δ . Despite this energy gap, it turns out that the edge states persist, as shown in Fig.2. It is natural to ask if these edge states in the presence of on-site interaction are topological in origin. If so, in what sense? Moreover, the Zak phase[20] of interacting armchair graphene nanoribbons is mod 2π , implying that the boundary charge may be zero or an integer[21, 22]. Considering these factors, it's not clear whether interacting graphene nanoribbons constitute a short-range entangled symmetry-protected topological insulator. (Here, we exclude consideration of disordered zigzag ribbons that exhibit long-range entangled topological order[19], as discussed in Ref. [12].)

We aim to address the aforementioned questions by investigating the interacting nanoribbons within the framework of the Hartree-Fock (HF) approach and employing an anomalous continuity equation similar to Eq. (6). The self-consistent HF fields break chiral symmetry. However, the self-consistent fields of the opposite zigzag edges exhibit antisymmetry under mirror symmetry operation. The relevant symmetry combines mirror and time-reversal operations, enabling the formation of a topological charge induced by the mass on ferromagnetic zigzag edges in undoped ribbons. This mechanism is analogous to the equation in Eq.(8). This topological charge persists even in the low-doped region where the ground state displays edge

spin density waves. It appears as a nearly zero energy edge mode. Our work demonstrates that interacting graphene nanoribbons retain their status as symmetry-protected topological insulators.

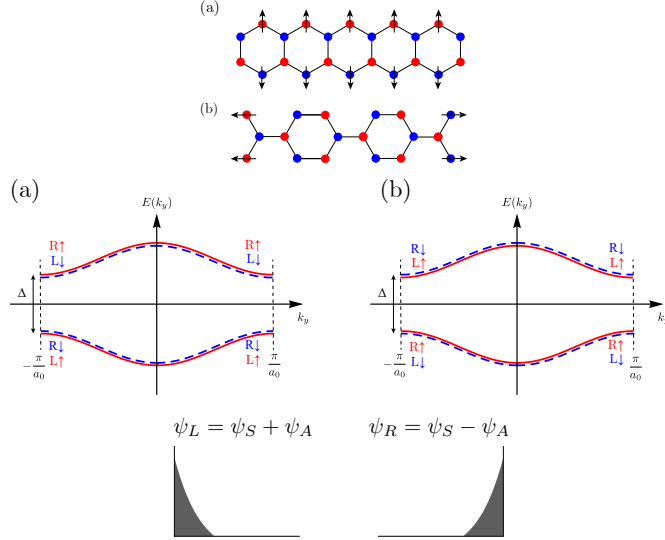


Figure 2: **First:** Two interacting rectangular nanoribbons are shown. A graphene zigzag nanoribbon (a) and an armchair nanoribbon (b) consist of two sublattices, A (red sites) and B (blue sites). In a zigzag (armchair) ribbon, the left and right carbon sites are part of the armchair (zigzag) edges. The net site spins of the zigzag edges are displayed. The spins are 'down' on the red 'A' sites and 'up' on the blue 'B' sites. Zigzag edges are antiferromagnetically coupled, while each of them is ferromagnetically ordered. Site spin values are determined by the occupation numbers $n_{i\sigma}$: $s_{iz} = \frac{1}{2}[n_{i\uparrow} - n_{i\downarrow}]$, where i denotes a site, and σ represents spin up or down. A edge sites are predominantly occupied by spin-down, while the B edge sites are predominantly occupied by the opposite spin. Therefore, in each sublattice, the total occupation numbers of spin-up and spin-down electrons are different. **Second:** Band structures of two degenerate ground states of a zigzag nanoribbon in the presence of on-site Coulomb repulsion. Zigzag edge states are found near the band gap edges, occurring at energies approximately $E \approx \pm\Delta/2$, with momenta around $k \approx \pm\pi/a_0$. L and R stand for left and right edge localized states. **Third:** Zigzag edge states ψ_L and ψ_R , exclusively localized on either the left or right edge, result from the combination of symmetric ψ_S and antisymmetric ψ_A solitonic states, as depicted in Fig.1.

2 Tight-binding Hubbard model of Nanoribbon

Let us consider the narrowest armchair nanoribbon with zigzag edges and the narrowest zigzag nanoribbon, as illustrated in the top figure of Fig. 2. The Hamiltonian of the tight-binding Hubbard model of these nanoribbons consists of the hopping term with hopping amplitude t and the Hubbard term for on-site Coulomb repulsion U

$$\hat{H} = \hat{H}_t + \hat{H}_U. \quad (11)$$

The second quantized hopping Hamiltonian is (h.c. is the Hermitian conjugate, and $\sigma = \uparrow, \downarrow$ is spin)

$$\hat{H}_t = -t \sum_{\langle \mathbf{R}, \mathbf{R}' \rangle \sigma} (\hat{c}_{\mathbf{R}\sigma}^\dagger \hat{c}_{\mathbf{R}'\sigma} + \text{h.c.}), \quad (12)$$

where $\hat{c}_{\mathbf{R},\sigma}$ is the electron destruction operator at site \mathbf{R} with spin σ and $\langle \mathbf{R}, \mathbf{R}' \rangle$ denotes a nearest-neighbor pair. One of the pair belongs to A-sublattice, while the other is in B-sublattice. The Hubbard term is given by

$$\hat{H}_U = U \sum_{\mathbf{R}} \hat{n}_{\mathbf{R}\uparrow} \hat{n}_{\mathbf{R}\downarrow}, \quad (13)$$

where $\hat{n}_{\mathbf{R}\sigma} = \hat{c}_{\mathbf{R}\sigma}^\dagger \hat{c}_{\mathbf{R}\sigma}$ is the electron number operator at site \mathbf{R} with spin σ . As discussed in Section 1, \hat{H}_t possesses the chiral symmetry, while the \hat{H}_U explicitly breaks it.

Applying HF mean-field theory to Eq.(13) at *half-filling*, a quadratic mean-field Hamiltonian \hat{H}_{HF} can be obtained:

$$\hat{H}_{\text{HF}} = \hat{H}_t + \hat{H}_{U,\text{HF}}, \quad \hat{H}_{U,\text{HF}} = \sum_{\mathbf{R}\sigma} \Delta_{\mathbf{R}\sigma} \hat{n}_{\mathbf{R}\sigma}, \quad (14)$$

where the gap parameter $\Delta_{\mathbf{R}\sigma}$, which corresponds to the mass parameter of Eq.(6), is defined by

$$\Delta_{\mathbf{R}\sigma} = U \left(\langle \hat{n}_{\mathbf{R}\bar{\sigma}} \rangle - \frac{1}{2} \right), \quad \bar{\sigma} = \text{the opposite spin of } \sigma. \quad (15)$$

A constant term has been added to \hat{H}_{HF} to make the Fermi energy to be zero. The site gap $\Delta_{\mathbf{R}\bar{\sigma}}$ associated with spin $\bar{\sigma}$ can be understood as the staggered potential energy for an electron with the opposite spin σ . This potential is staggered since it changes sign between A- and B-sites, as depicted in Fig. 4. It is important to note that the mean-field HF Hamiltonian can be split into the spin-up and the spin-down components [23]:

$$\hat{H}_{\text{HF}} = \hat{H}_{\text{HF}\uparrow} + \hat{H}_{\text{HF}\downarrow}. \quad (16)$$

The band structure *without* the Hubbard interaction \hat{H}_U taken into account was shown in Fig.1[24, 25]. The nearly zero-energy edge states exist close to the Brillouin zone boundary, and they exhibit non-magnetic behavior (the net spin polarization of a zigzag edge is zero). The existence of these *zero* energy chiral edge states crucially rests on the chiral symmetry. However, a self-consistent solution of the HF mean-field Hamiltonian reveals that for ribbon widths shorter than 100 Å, the ground state is antiferromagnetic. In this state, site spins of sublattice A (B) are spin-up (-down), and the state is doubly degenerate with an energy gap, as mentioned in references [26, 27]. The HF results[28] qualitatively agree with those of density matrix renormalization methods[29] and ab initio calculations[30]. The chiral edge states *do* exist, and these chiral edge states are now oppositely polarized (edge antiferromagnetism) [26]. Each zigzag edge displays ferromagnetism but the opposite zigzag edges with different chirality are antiferromagnetically coupled (see the top figure of Fig. 2). The band structures are displayed in the second figure in Fig. 2.

3 Symmetry of undoped rectangular ribbons

Ribbons exhibit a symmetry based on the combined operation of parity transformation (mirror reflection) and time reversal transformations, as described by the relationship:

$$\langle \hat{n}_{\mathbf{R}\sigma} \rangle = \langle \hat{n}_{\bar{\mathbf{R}}\bar{\sigma}} \rangle. \quad (17)$$

This relation is illustrated in Fig.3. Note that $\bar{\mathbf{R}}$ is the mirror symmetric site of \mathbf{R} and $\bar{\sigma}$ is the opposite spin of σ . Here, the relevant mirror axis of the zigzag nanoribbon is the *horizontal* x-axis and that of the armchair nanoribbon the *vertical* y-axis through the center of the ribbon. This symmetry aligns with the existence of a spin-up edge state on one zigzag edge and the corresponding spin-down edge state on the opposite zigzag edge.

Then the definition of the gap parameter Eq.(15) immediately implies that

$$\Delta_{\mathbf{R}\sigma} = U \left(\langle \hat{n}_{\mathbf{R}\sigma} \rangle - \frac{1}{2} \right) = U \left(\langle \hat{n}_{\bar{\mathbf{R}}\bar{\sigma}} \rangle - \frac{1}{2} \right) = \Delta_{\bar{\mathbf{R}}\bar{\sigma}}. \quad (18)$$

Note that Eq.(18) is valid even for the low-doped case as long as Eq.(17) is valid. It is important to note that this mirror symmetry is accompanied by spin reversal and that the symmetry in the occupation numbers involves a spin reversal but not in the site gap values. At half-filling (undoped case),

the condition $\langle \hat{n}_{\mathbf{R}\sigma} \rangle + \langle \hat{n}_{\mathbf{R}\bar{\sigma}} \rangle = 1$ being combined with Eq.(17) yields

$$\Delta_{\mathbf{R}\sigma} = -\Delta_{\mathbf{R}\bar{\sigma}}, \quad (19)$$

which is demonstrated in Fig. 4.

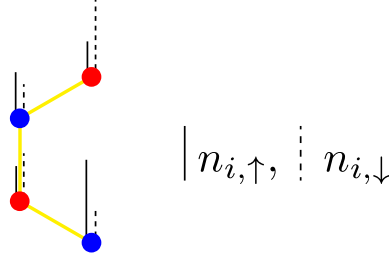


Figure 3: The values of $n_{i,\uparrow}$ (represented by vertical solid lines) and $n_{i,\downarrow}$ (shown as vertical dashed lines) within a unit cell of the shortest-width zigzag ribbon are depicted. Note that for each site $\langle n_{\mathbf{R},\uparrow} \rangle + \langle n_{\mathbf{R},\downarrow} \rangle = 1$.

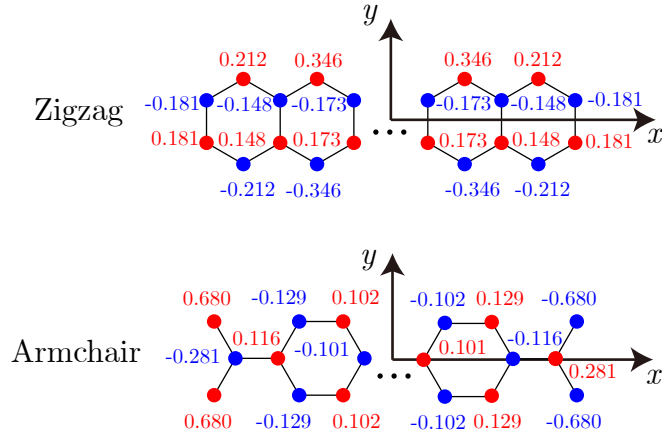


Figure 4: Magnitude of the self-consistent gap $\Delta_{\mathbf{R}\uparrow}$ at each site. Mirror symmetry about the horizontal (vertical) axis is present only in the armchair (zigzag) case. We will call these axes the mirror axes. Note that *only up-spin* gap parameters are indicated.

4 Symmetry of low-doped zigzag ribbons

Let us consider zigzag ribbons in the low doping limit. It turns out that doping has a singular effect[29]: the ground state displays an edge spin density wave, as shown in Fig.5. This is in contrast to the uniform edge ferromagnetism of the half-filled case. Note that in the low-doped region, the electron spins are collinear to a very good approximation, as confirmed by the density matrix renormalization group approach in the matrix product representation. This implies that our Hamiltonian at half-filling may still be applicable[29].

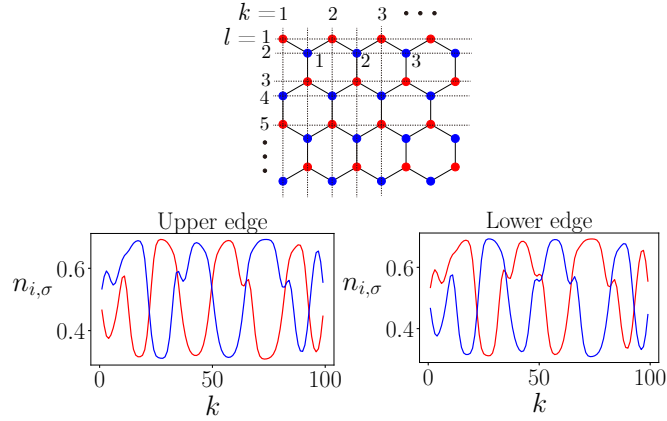


Figure 5: Spin-up and spin-down profiles of $\langle n_{\mathbf{R},\sigma} \rangle$ at the zigzag edges of a doped zigzag ribbon with an additional $\delta N = 12$ electrons added to half-filling. Note that $\langle n_{\mathbf{R},\uparrow} \rangle + \langle n_{\mathbf{R},\downarrow} \rangle \neq \text{constant}$, i.e., it varies from site to site. The site spins $s_{\mathbf{R},z} = \frac{1}{2}[\langle n_{\mathbf{R},\uparrow} \rangle - \langle n_{\mathbf{R},\downarrow} \rangle]$ of the upper edge is out of phase with that of the lower edge. The site \mathbf{R} is parametrized by (k, l) .

To understand the role of the doping we write the filling condition as

$$\langle \hat{n}_{\mathbf{R}\sigma} \rangle + \langle \hat{n}_{\mathbf{R}\bar{\sigma}} \rangle = 1 + \delta, \quad (20)$$

where δ is the doping level. Then we have

$$\Delta_{\mathbf{R}\sigma} = U \left(\langle \hat{n}_{\mathbf{R}\bar{\sigma}} \rangle - \frac{1}{2} \right) = U \left(1 + \delta - \langle \hat{n}_{\mathbf{R}\sigma} \rangle - \frac{1}{2} \right) = -\Delta_{\mathbf{R}\bar{\sigma}} + U\delta = -\Delta_{\bar{\mathbf{R}}\sigma} + U\delta. \quad (21)$$

Eq.(21) shows that the antisymmetry of the gap parameter $\Delta_{\mathbf{R}\sigma}$ observed at half-filling in Fig. 4 is disrupted when moving away from the half-filling state relative to the mirror axis.

5 Anomalous continuity equation

The total current operator of the tight-binding Hamiltonian Eq.(11) is given by

$$\mathbf{J}_{\text{tot}} = it \sum_{\langle \mathbf{R}, \mathbf{R}' \rangle, \sigma} (\mathbf{R} - \mathbf{R}') (\hat{c}_{\mathbf{R}, \sigma}^\dagger \hat{c}_{\mathbf{R}', \sigma} - \text{h.c.}), \quad (22)$$

which is defined such that the ordinary continuity equation is satisfied. Remember, in one-dimensional Dirac fermions, the axial current can be defined, where the roles of charge density ρ and spatial charge current density j interchange between ordinary and axial current (as shown in Eq.(2)). Additionally, the Frölich equation governing the (unpinned) sliding charge density wave [31] is expressed as:

$$\nabla \rho + \frac{1}{v_F^2} \frac{\partial j}{\partial t} = \kappa E. \quad (23)$$

Here, κ represents compressibility, v_F signifies Fermi velocity, and E denotes an electric field. In one-dimensional systems, Eq.(23) essentially embodies the well-known axial anomaly[2]. These insights lead us to consider the *time derivative* of the spatial current, as outlined in Eq.(22). This approach is motivated by the pronounced manifestation of chiral (axial) symmetry breaking effects, notably evident in the continuity equation for the axial current (Eq.(6)).

The time derivative can be found from the commutator with \hat{H}_{HF} Eq.(14):

$$\frac{\partial \mathbf{J}_{\text{tot}}}{\partial t} = \frac{i}{\hbar} [\hat{H}_{U, \text{HF}}, \mathbf{J}_{\text{tot}}] + \frac{i}{\hbar} [\hat{H}_t, \mathbf{J}_{\text{tot}}]. \quad (24)$$

This expression comprises two contributions: one from the HF decomposed Hubbard interaction and the other from the hopping term. Taking the HF ground state expectation value of Eq.(24) and considering the temporal adiabatic limit, $(-i\hbar) \frac{\partial \langle \mathbf{J}_{\text{tot}} \rangle}{\partial t} \approx 0$ we find :

$$(-i\hbar) \frac{\partial \langle \mathbf{J}_{\text{tot}} \rangle}{\partial t} = \langle [\hat{H}_{U, \text{HF}}, \mathbf{J}_{\text{tot}}] \rangle + \langle [\hat{H}_t, \mathbf{J}_{\text{tot}}] \rangle \approx 0. \quad (25)$$

Then, we explore the implications of Eq.(25) in light of the (integrated) anomalous continuity equation (Eq.(6)) and the accumulation of the topological charge (Eq.(8)).

The computation of the commutators are straightforward. For each spin projection, we find

$$[\hat{H}_{U, \text{HF}}, \mathbf{J}_{\text{tot}, \sigma}] = (+i)t \sum_{\langle \mathbf{R}, \mathbf{R}' \rangle} (\mathbf{R} - \mathbf{R}') (\Delta_{\mathbf{R}\sigma} - \Delta_{\mathbf{R}'\sigma}) (\hat{c}_{\mathbf{R}, \sigma}^\dagger \hat{c}_{\mathbf{R}'\sigma} + \text{h.c.}), \quad (26)$$

and

$$[\hat{H}_t, \mathbf{J}_{\text{tot},\sigma}] = (-i)t^2 \sum_{\langle \mathbf{R}_1, \mathbf{R} \rangle} \sum_{\langle \mathbf{R}, \mathbf{R}' \rangle} (\mathbf{R} - \mathbf{R}') (\hat{c}_{\mathbf{R}_1\sigma}^\dagger \hat{c}_{\mathbf{R}'\sigma} + \text{h.c.}). \quad (27)$$

It's important to clarify that in Eq.(27), \mathbf{R}_1 and \mathbf{R}' are *not* a nearest neighbor pair, see Fig.6. To elaborate further, if we consider a fixed \mathbf{R}' , then \mathbf{R} must be a nearest neighbor in the other sublattice, thereby determining the bond vector $\mathbf{R} - \mathbf{R}'$. Subsequently, \mathbf{R}_1 should be a nearest neighbor of \mathbf{R} , placing it in the same sublattice as \mathbf{R}' . Now, considering the proximity of \mathbf{R}' to \mathbf{R} , \mathbf{R}_1 *can* be \mathbf{R}' , resulting in $\hat{c}_{\mathbf{R}'\sigma}^\dagger \hat{c}_{\mathbf{R}'\sigma} + \text{h.c.}$, effectively representing two times the number operator at \mathbf{R}' . However, it's crucial to note that \mathbf{R}_1 might not necessarily be the same as \mathbf{R}' ; in such cases, \mathbf{R}_1 becomes a next-nearest neighbor site from \mathbf{R}' while still being in the same sublattice. Thus, Eq.(27) can be expressed as

$$[\hat{H}_t, \mathbf{J}_{\text{tot},\sigma}] = (-i)2t^2 \sum_{\mathbf{R}'} \sum_{\langle \mathbf{R}, \mathbf{R}' \rangle} (\mathbf{R} - \mathbf{R}') \hat{n}_{\mathbf{R}'\sigma} + \text{next-nearest bond terms}. \quad (28)$$

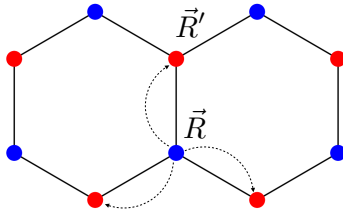


Figure 6: The possible locations of sites represented by \mathbf{R}_1 are indicated by dashed lines.

Some examples of the next-nearest bond terms can be visualized using Fig. 7, such as $\langle \hat{c}_{l+1,3,\uparrow}^\dagger \hat{c}_{l,1,\uparrow} \rangle$. We note that in the framework of the anomalous continuity equation treated here, no bonds longer than the next-nearest ones appear.

It is important to emphasize that these results describe *two*-dimensional electron motion, covering the charge movement both along and perpendicular to the ribbon. In the following section we apply the above results to the zigzag nanoribbons depicted in the top figure of Fig. 2.

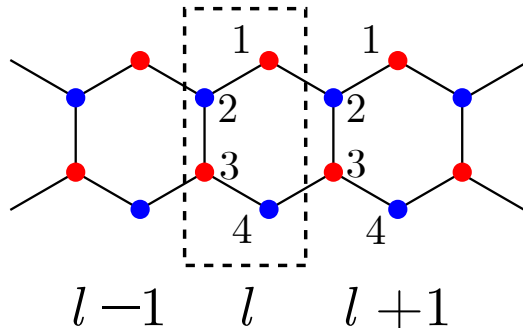


Figure 7: Unit cells of a zigzag ribbon are labeled by index l .

6 Topological charge of zigzag edges

In consideration of the anomalous continuity equation of the axial current (Eq.(6)), we must compute the expectation value of the gap term (Eq.(26)) and the terms originating from the hopping Hamiltonian (Eq.(28)) concerning the HF ground state. Recalling that the HF Hamiltonian is split into the spin-up and the spin-down components (see Eq.(16)) the expectation values can be computed for each spin component separately.

Now it is crucial to note that there is a *vertical mirror axis* through the center of the zigzag ribbon (see Fig.4). Then the expectation values of the bond operators of Eqs.(26,28) should respect this mirror symmetry. We hasten to comment that this mirror symmetry operation does *not* involve spin reversal. However, the mirror symmetry employed in the discussion of the gap parameter in Section 3 does involve spin reversal. Therefore, these two mirror symmetry operations are distinct from each other.

This vertical mirror symmetry implies that the horizontal x-component of the expectation values of the operators of Eqs.(26,28) vanish identically owing to the oddness of the horizontal component of the bond vector $\mathbf{R} - \mathbf{R}'$ of Eqs.(26,28) under the mirror reflection, so that the topological charges can be accumulated only along the vertical direction: the upper and the lower chiral zigzag edges. Below l, m denote the unit cell and the position within the unit cell, respectively (see Fig. 7).

For simplicity, we'll evaluate the axial current for the smallest-width zigzag nanoribbons. Subsequently, we will validate this result for larger

widths. This model of zigzag nanoribbons will clearly reveal the main physics. Firstly, regarding the expectation value of the hopping Hamiltonian in Eq.(28), it comprises two distinct components. Initially, we focus on the first term, the contribution stemming from the density operator terms. We observe that the contributions from $m = 2$ and $m = 3$ sites (refer to Fig.7) vanish. This occurs due to the vertical components of the nearest bond vector emanating from the site, summing up to zero. Thus, only the upper and lower edge sites contribute to the summation for the vertical y-component in the first term of Eq.(28). This yields:

$$[\widehat{H}_t, \mathbf{J}_{\text{tot},\sigma}] = (-2i)(t^2 \sum_{\mathbf{R}'} \sum_{\langle \mathbf{R}, \mathbf{R}' \rangle} (\mathbf{R} - \mathbf{R}')_y \widehat{n}_{\mathbf{R}'\sigma}) = 2it^2 a \sum_l \left(\langle \widehat{n}_{l,1,\sigma} \rangle - \langle \widehat{n}_{l,4,\sigma} \rangle \right). \quad (29)$$

For edge states that are well-localized on the zigzag edges this result is exactly the structure anticipated from Eq.(8), namely only the boundary contributions remain. Now, we estimate the second term of Eq.(28), consisting of next-nearest bond contributions. It may be ignored. This is because the next-nearest bond terms are small when the distance between these bonds, $|\mathbf{R} - \mathbf{R}'|$, exceeds the correlation length ξ . Note that the one-particle correlation function, expressed as:

$$C_\sigma(\mathbf{R}, \mathbf{R}') = \langle c_{\mathbf{R}\sigma}^\dagger c_{\mathbf{R}'\sigma} \rangle \quad (30)$$

remains significant only within the correlation length. As U increases, Δ also rises, leading to a decrease in the correlation length $\xi \sim \hbar v_F / \Delta$ (where v_F represents the velocity of Dirac electrons).

The expectation value of the vertical component of the gap parameter contribution Eq.(26) is found to be

$$\begin{aligned} \langle [\widehat{H}_{U,\text{HF}}, \mathbf{J}_{\text{tot},\sigma}] \rangle_y &= -ita \sum_l \left[\frac{1}{2} (\Delta_{l,2,\sigma} - \Delta_{l,1,\sigma}) \langle \widehat{c}_{l,2,\sigma}^\dagger \widehat{c}_{l,1,\sigma} + \text{h.c.} \rangle \right. \\ &+ (\Delta_{l,3,\sigma} - \Delta_{l,2,\sigma}) \langle \widehat{c}_{l,3,\sigma}^\dagger \widehat{c}_{l,2,\sigma} + \text{h.c.} \rangle + \frac{1}{2} (\Delta_{l,4,\sigma} - \Delta_{l,3,\sigma}) \langle \widehat{c}_{l,4,\sigma}^\dagger \widehat{c}_{l,3,\sigma} + \text{h.c.} \rangle \\ &+ \frac{1}{2} (\Delta_{l+1,2,\sigma} - \Delta_{l,1,\sigma}) \langle \widehat{c}_{l+1,2,\sigma}^\dagger \widehat{c}_{l,1,\sigma} + \text{h.c.} \rangle \\ &\left. + \frac{1}{2} (\Delta_{l,4,\sigma} - \Delta_{l+1,3,\sigma}) \langle \widehat{c}_{l,4,\sigma}^\dagger \widehat{c}_{l+1,3,\sigma} + \text{h.c.} \rangle \right]. \quad (31) \end{aligned}$$

The site numbers of the unit cell used in this equation are defined in Fig.7. For a ribbon with a large number of unit-cells, the expectation values of the nearest-neighbor bond operators will be identical between unit cells. Next let us focus $m = 3$ site. In the presence of translational symmetry the expectation values of bond operator with $m = 4$ site in the l -th and the $l-1$

cells are identical. Then, the sum of the nearest-neighbor bond expectation values connected to $m = 3$ site in the l -th unit cell takes the following form:

$$\text{sum} = \Delta_{l,3,\sigma} \left(\langle \hat{c}_{l,3,\sigma}^\dagger \hat{c}_{l,2,\sigma} + \text{h.c.} \rangle - 2 \times \frac{1}{2} \langle \hat{c}_{l,4,\sigma}^\dagger \hat{c}_{l,3,\sigma} + \text{h.c.} \rangle \right). \quad (32)$$

Our numerical evaluation shows that, for $U \gg 2t$, the correlation function values satisfy:

$$\langle \hat{c}_{l,1,\sigma}^\dagger \hat{c}_{l,2,\sigma} \rangle \approx \langle \hat{c}_{l,2,\sigma}^\dagger \hat{c}_{l,3,\sigma} \rangle \approx \langle \hat{c}_{l,3,\sigma}^\dagger \hat{c}_{l,4,\sigma} \rangle. \quad (33)$$

We thus find that the difference between the two expectation values of bonds in Eq.(32) is small. This means that the contribution of the gap parameter $\Delta_{l,3,\sigma}$ will be negligible. The same argument can be applied to the $m = 2$ site, too.

Therefore, the result Eq.(31) simplifies to

$$\langle [\hat{H}_{U,\text{HF}}, \mathbf{J}_{\text{tot},\sigma}] \rangle|_y \approx -ita\mathcal{B} \left(\sum_l (\Delta_{l,4,\sigma} - \Delta_{l,1,\sigma}) \right), \quad (34)$$

where \mathcal{B} denotes the expectation value of the nearest-neighbor bond operator (as given in Eq.(33)) plus its hermitian conjugate. The simplified result Eq.(34) tells us that the contributions from the upper and the lower zigzag edges are dominant. Now employing the temporal adiabatic condition Eq.(25),

$$\langle [\hat{H}_t, \mathbf{J}_{\text{tot},\sigma}] \rangle|_y = -\langle [\hat{H}_{U,\text{HF}}, \mathbf{J}_{\text{tot},\sigma}] \rangle|_y \quad (35)$$

we arrive at

$$\sum_l \left(\langle \hat{n}_{l,1,\sigma} \rangle - \langle \hat{n}_{l,4,\sigma} \rangle \right) \approx \frac{\mathcal{B}}{2t} \sum_l \left(\Delta_{l,4,\sigma} - \Delta_{l,1,\sigma} \right). \quad (36)$$

We have numerically verified the correctness of this result for various widths, as depicted in Fig. 8. The observations from this figure suggest that the topological charge remains well-defined for $\Delta/2 \gtrsim t$ (occurring when $U \gtrsim 3t$), indicating that the self-consistent staggered potential, as described in Eq.(15), obstructs electron hopping, resulting in stronger localization on the zigzag edges. When the terms from the next-nearest bonds are added to the right side of Eq.(36), there is an almost exact agreement with the left side.

The above result explicitly demonstrates that the edge occupations of the zigzag nanoribbons are determined by the values of the gap parameters in the vicinity of the edge. This allows us to recognize the edge occupations of the zigzag nanoribbons as a topological charge linked to the solitonic behavior of the gap parameters. This identification parallels Eq.(8), which

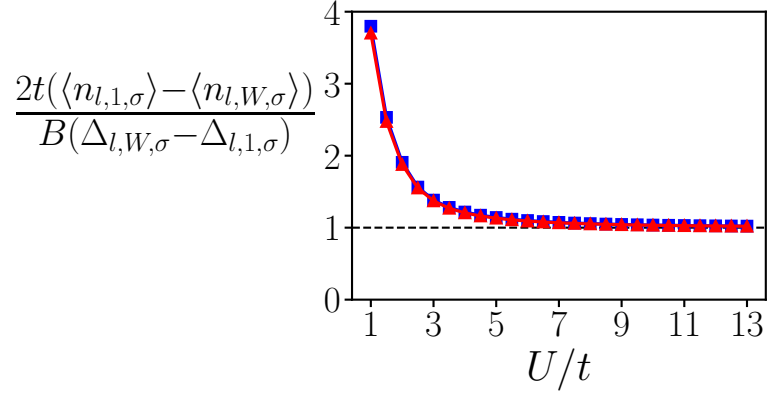


Figure 8: Numerical tests were conducted to validate the analytical result given in Eq.(36) for two distinct ribbon widths: $W = 4$ and 8 (these widths are defined in Fig.5). The horizontal dashed line is the expected value for large U .

associates the induced fermion numbers with the topological charge of a soliton.

So far we have investigated the topological charges of zigzag ribbons. It turns out that a rectangular armchair ribbon may also support topological edge states because it has two zigzag edges. As the ribbon width increases more topological edge states are formed in the gap, as shown in Fig.9.

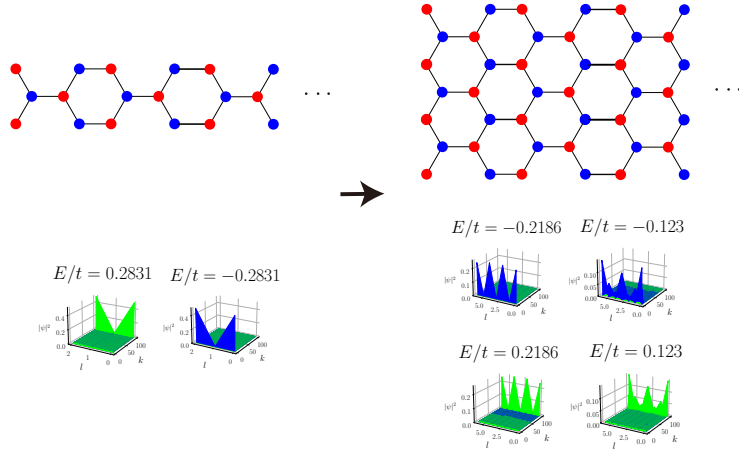


Figure 9: Plot of zigzag edge state probability density of undoped rectangular ribbons. As the ribbon width increases more nearly zero energy states are created in the gap.

We investigate whether low-doped ribbons, characterized by the edge spin density ground state, possess topological edge states. Our numerical studies reveal that within the low-doped region, the ribbon hosts nearly zero-energy gap states with a topological charge, as illustrated in Fig. 10. However, it's important to note that in the undoped case, the edge states have energies around $E \approx \pm\Delta/2$, as depicted in Fig. 2.

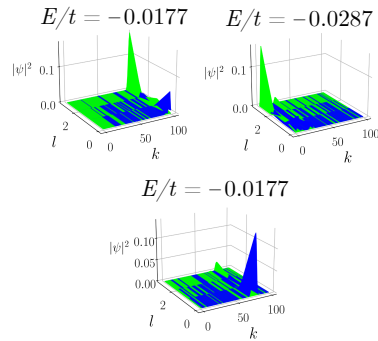


Figure 10: Occupied spin-up zigzag edge states of a doped ribbon $\delta N = 12$. There are also similar spin-down states. Here $U = 2t$.

7 Discussion and Summary

Our findings suggest that chiral symmetry breaks due to on-site repulsion among electrons. However, an abrupt spatial change in the gap at the zigzag edges enables the emergence of topological charges with energies around $\pm\Delta/2$, leading to the formation of a symmetry-protected topological insulator. This symmetry is dependent on combined operations involving parity (mirror reflection) and time reversal transformations. In contrast, despite a significant gap change at the armchair edges, no topological charges are formed in those regions.

In low-doped ribbons, the ground state forms an edge spin density wave rather than a ferromagnetic edge. This state supports nearly zero-energy zigzag edge states, distinct from the $\pm\Delta/2$ energies, exhibiting a gap-induced topological charge.

We hope that our work will stimulate the study of atomically precise nanoribbons recently fabricated [7, 8] from the perspective of symmetry-protected topological insulators. It would be intriguing to observe topological charges of nearly zero energy states in low-doped ribbons that exhibit the edge spin-density wave ground state. Scanning tunneling microscopy[32] could be employed for this purpose.

Appendices

For a precise description let us introduce Dirac Hamiltonian. The the classical Lagrangian density of the gapless Dirac fermion in the presence U(1) gauge potential A_μ is given by (Einstein summation convention assumed)

$$\mathcal{L} = \bar{\psi}i\gamma^\mu(\partial_\mu + ieA_\mu)\psi, \quad \bar{\psi} = \psi^\dagger\gamma^0, \quad (37)$$

where the spacetime indices μ, ν take the value 0, 1 for time t and space x , respectively. The gamma matrices are defined by

$$\{\gamma^\mu, \gamma^\nu\} = 2g^{\mu\nu} = 2 \begin{pmatrix} 1 & 0 \\ 0 & -1 \end{pmatrix}, \quad \mu = 0, 1 \quad (38)$$

$$\gamma^0 = \begin{pmatrix} 0 & -i \\ i & 0 \end{pmatrix}, \quad \gamma^1 = \begin{pmatrix} 0 & i \\ i & 0 \end{pmatrix} = i\sigma_x, \quad \gamma^5 = \gamma^0\gamma^1 = \begin{pmatrix} 1 & 0 \\ 0 & -1 \end{pmatrix} \quad (39)$$

The representation of gamma matrices where γ^5 is diagonal is called the *chiral representation*, so Eq.(38) is a chiral representation.

Writing (R, L denotes the handedness)

$$\psi = \begin{pmatrix} \psi_R \\ \psi_L \end{pmatrix}, \quad (40)$$

the Lagrange equations of motion in the absence of the gauge field yield

$$(\partial_0 + \partial_1)\psi_R = 0, \quad (\partial_0 - \partial_1)\psi_L = 0, \quad (41)$$

which implies that the right handed fermion is right moving, and vice versa.

The eigenvalue of γ^5 is defined to be the chirality, and the following properties of γ^5 play an important role:

$$\{\gamma^5, \gamma^\mu\} = 0, \quad \gamma^\mu \gamma^5 = -\epsilon^{\mu\nu} \gamma_\nu, \quad \epsilon^{01} = +1 \quad (42)$$

where $\epsilon^{\mu\nu}$ is a totally antisymmetric tensor and $\gamma_0 = \gamma^0, \gamma_1 = -\gamma^1$.

References

- [1] Jeffrey Goldstone and Frank Wilczek. “Fractional Quantum Numbers on Solitons”. Phys. Rev. Lett. 47 (14 1981), pp. 986–989. DOI: [10.1103/PhysRevLett.47.986](https://doi.org/10.1103/PhysRevLett.47.986).
- [2] E. Fradkin. Quantum Field Theory: An Integrated Approach. Princeton University Press, 2021. ISBN: 9780691189550.
- [3] R. Jackiw and C. Rebbi. “Solitons with fermion number 1/2”. Phys. Rev. D 13 (12 1976), p. 3398. DOI: [10.1103/PhysRevD.13.3398](https://doi.org/10.1103/PhysRevD.13.3398).
- [4] A. J. Heeger et al. “Solitons in conducting polymers”. Rev. Mod. Phys. 60 (3 1988), pp. 781–850. DOI: [10.1103/RevModPhys.60.781](https://doi.org/10.1103/RevModPhys.60.781).
- [5] Steven M Girvin and Kun Yang. Modern condensed matter physics. Cambridge: Cambridge University Press, 2019. DOI: [10.1017/9781316480649](https://doi.org/10.1017/9781316480649).
- [6] Jianis K Pachos. Introduction to Topological Quantum Computation. Cambridge: Cambridge University Press, 2012. DOI: [10.1017/CB09780511792908](https://doi.org/10.1017/CB09780511792908).
- [7] Pascal Ruffieux et al. “On-surface synthesis of graphene nanoribbons with zigzag edge topology”. Nature 531.7595 (2016), pp. 489–492. DOI: [10.1038/nature17151](https://doi.org/10.1038/nature17151).
- [8] Marek Kolmer et al. “Rational synthesis of atomically precise graphene nanoribbons directly on metal oxide surfaces”. Science 369.6503 (2020), pp. 571–575. DOI: [10.1126/science.abb8880](https://doi.org/10.1126/science.abb8880).

- [9] R. S. Koen Houtsma, Joris de la Rie, and Meike Stöhr. “Atomically precise graphene nanoribbons: interplay of structural and electronic properties”. *Chem. Soc. Rev.* 50 (11 2021), pp. 6541–6568. DOI: [10.1039/D0CS01541E](https://doi.org/10.1039/D0CS01541E).
- [10] A. H. Castro Neto et al. “The electronic properties of graphene”. *Rev. Mod. Phys.* 81 (1 2009), pp. 109–162. DOI: [10.1103/RevModPhys.81.109](https://doi.org/10.1103/RevModPhys.81.109).
- [11] Luis Brey, Pierre Seneor, and Antonio Tejeda, eds. *Graphene Nanoribbons*. 2053-2563. IOP Publishing, 2019. ISBN: 978-0-7503-1701-6. DOI: [10.1088/978-0-7503-1701-6](https://doi.org/10.1088/978-0-7503-1701-6).
- [12] S.-R. Eric Yang. *Topologically Ordered Zigzag Nanoribbon*. World Scientific, Singapore, 2023. DOI: [10.1142/13013](https://doi.org/10.1142/13013).
- [13] S.-R. Eric Yang. “Soliton fractional charges in graphene nanoribbon and polyacetylene: similarities and differences”. *Nanomaterials* 9.6 (2019), p. 885. DOI: [10.3390/nano9060885](https://doi.org/10.3390/nano9060885).
- [14] Shinsei Ryu and Yasuhiro Hatsugai. “Topological Origin of Zero-Energy Edge States in Particle-Hole Symmetric Systems”. *Phys. Rev. Lett.* 89 (7 2002), p. 077002. DOI: [10.1103/PhysRevLett.89.077002](https://doi.org/10.1103/PhysRevLett.89.077002).
- [15] P. Delplace, D. Ullmo, and G. Montambaux. “Zak phase and the existence of edge states in graphene”. *Phys. Rev. B* 84 (19 2011), p. 195452. DOI: [10.1103/PhysRevB.84.195452](https://doi.org/10.1103/PhysRevB.84.195452).
- [16] Ken ichi Sasaki et al. “Soliton trap in strained graphene nanoribbons”. *New Journal of Physics* 12.10 (2010), p. 103015. DOI: [10.1088/1367-2630/12/10/103015](https://doi.org/10.1088/1367-2630/12/10/103015).
- [17] YH Jeong, SC Kim, and S-R Eric Yang. “Topological gap states of semiconducting armchair graphene ribbons”. *Physical Review B* 91.20 (2015), p. 205441.
- [18] Jiannis K. Pachos. “Manifestations of topological effects in graphene”. *Contemporary Physics* 50.2 (2009), pp. 375–389. DOI: [10.1080/00107510802650507](https://doi.org/10.1080/00107510802650507).
- [19] Xiao-Gang Wen. “Colloquium: Zoo of quantum-topological phases of matter”. *Rev. Mod. Phys.* 89 (4 2017), p. 041004. DOI: [10.1103/RevModPhys.89.041004](https://doi.org/10.1103/RevModPhys.89.041004).
- [20] J. Zak. “Berry’s phase for energy bands in solids”. *Phys. Rev. Lett.* 62 (23 1989), pp. 2747–2750. DOI: [10.1103/PhysRevLett.62.2747](https://doi.org/10.1103/PhysRevLett.62.2747).
- [21] David Vanderbilt and R. D. King-Smith. “Electric polarization as a bulk quantity and its relation to surface charge”. *Phys. Rev. B* 48 (7 1993), pp. 4442–4455. DOI: [10.1103/PhysRevB.48.4442](https://doi.org/10.1103/PhysRevB.48.4442).

- [22] Y.H. Jeong and S.-R. Eric Yang. “Topological end states and Zak phase of rectangular armchair ribbon”. *Annals of Physics* 385 (2017), pp. 688–694. ISSN: 0003-4916. DOI: <https://doi.org/10.1016/j.aop.2017.08.019>.
- [23] S.-R. Eric Yang et al. “Topologically ordered zigzag nanoribbon: $e/2$ fractional edge charge, spin-charge separation, and ground-state degeneracy”. *Phys. Rev. Research* 2 (3 2020), p. 033109. DOI: [10.1103/PhysRevResearch.2.033109](https://doi.org/10.1103/PhysRevResearch.2.033109).
- [24] L. Brey and H. A. Fertig. “Electronic states of graphene nanoribbons studied with the Dirac equation”. *Phys. Rev. B* 73 (23 2006), p. 235411. DOI: [10.1103/PhysRevB.73.235411](https://doi.org/10.1103/PhysRevB.73.235411).
- [25] Shi-Hua Tan, Li-Ming Tang, and Ke-Qiu Chen. “Band gap opening in zigzag graphene nanoribbon modulated with magnetic atoms”. *Current Applied Physics* 14.11 (2014), pp. 1509–1513. ISSN: 1567-1739. DOI: <https://doi.org/10.1016/j.cap.2014.08.018>.
- [26] Mitsutaka Fujita et al. “Peculiar Localized State at Zigzag Graphite Edge”. *J. Phys. Soc. Jpn.* 65.7 (1996), pp. 1920–1923. DOI: [10.1143/JPSJ.65.1920](https://doi.org/10.1143/JPSJ.65.1920).
- [27] L. Pisani et al. “Electronic structure and magnetic properties of graphitic ribbons”. *Phys. Rev. B* 75 (6 2007), p. 064418. DOI: [10.1103/PhysRevB.75.064418](https://doi.org/10.1103/PhysRevB.75.064418).
- [28] T. Stauber et al. “Interacting Electrons in Graphene: Fermi Velocity Renormalization and Optical Response”. *Phys. Rev. Lett.* 118 (26 2017), p. 266801. DOI: [10.1103/PhysRevLett.118.266801](https://doi.org/10.1103/PhysRevLett.118.266801).
- [29] Young Heon Kim et al. “New disordered anyon phase of doped graphene zigzag nanoribbon”. *Scientific Reports* 12 (11 2022), p. 14551. DOI: [10.1038/s41598-022-18731-6](https://doi.org/10.1038/s41598-022-18731-6).
- [30] Li Yang et al. “Quasiparticle Energies and Band Gaps in Graphene Nanoribbons”. *Phys. Rev. Lett.* 99 (18 2007), p. 186801. DOI: [10.1103/PhysRevLett.99.186801](https://doi.org/10.1103/PhysRevLett.99.186801).
- [31] G. Frölich. “On the theory of superconductivity: the one-dimensional case”. *Proc. R. Soc. A* 223 (1154 1954), p. 296. DOI: [10.1098/rspa.1954.0116](https://doi.org/10.1098/rspa.1954.0116).
- [32] Eva Y Andrei, Guohong Li, and Xu Du. “Electronic properties of graphene: a perspective from scanning tunneling microscopy and magnetotransport”. *Reports on Progress in Physics* 75.5 (2012), p. 056501. DOI: [10.1088/0034-4885/75/5/056501](https://doi.org/10.1088/0034-4885/75/5/056501).